Fully Programmable MEMS Ciliary Actuator Arrays for Micromanipulation Tasks

J. W. Suh*	R. B. Darling	K.-F. Böhringer	B. R. Donald	H. Baltes	G. T. Kovacs
Xerox PARC	U. of Washington	U. of Washington	Dartmouth	ETH Zürich	Stanford
Coyote Hill Rd.	El. Engineering	El. Engineering	Computer Science	El. Engineering	El. Engineering
Palo Alto, CA	Seattle, WA	Seattle, WA	Hanover, NH	Zürich, CH	Stanford, CA

Abstract

The first micromachined bimorph organic ciliary array with on-chip CMOS circuitry is presented. This device is composed of an 8×8 *array of cells each having four orthogonally oriented actuators in an overall die size of* 9.4mm $\times$ 9.4mm. *The polyimide based actuators were fabricated directly above the selection and drive circuitry. Selection and activation of actuators in this array shows that integration was successful.*

The integration of CMOS electronics and MEMS micromechanisms allows the implementation of new task-level micromanipulation strategies. New low-level control algorithms (actuator gaits) were also demonstrated.

The array was programmed to perform several kinds of manipulation tasks, including linear translation, diagonal motion, as well as vector field operations such as squeeze field and radial field orienting and centering. Preliminary experiments were also performed with the first implementation of a "universal field" that uniquely positions and orients any non-symmetric part without programming or sensor feedback. All tasks were demonstrated using thin silicon dice of about 3mm $\times$ 3mm $\times$ 0.5mm *size as the object being moved.*

1 Introduction

One of the potential applications of MEMS actuators is in the moving and positioning of small parts because the actuators themselves are on a similar scale. Toward the realization of this goal, researchers have been designing and building arrayed actuator systems that can overcome some of the inherent limitations of most microactuators (limited range of motion, degrees of freedom, and force output) through the arrangement of actuators in series or parallel. A variety of actuation methods have been used including air jets [19, 11, 17, 12], electromagnetic actuators [13, 14, 18], piezoelectric actuators [10], electrostatic actuators [4], and thermal bimorph actuators [22, 1, 21]. Whatever the chosen actuation method, the actuators have two fundamental requirements: (1) the generation of enough force or torque to move not only themselves, but also to move external objects and (2) the generation of large displacements of the moving parts or of the media in which the parts move (e.g., air jets). The previously reported ciliary arrays [21] were, to our knowledge, the first ones able to move small parts in a controlled and repeatable manner along any user-chosen direction in an x-y plane. This paper presents the first cilia micromanipulator array with fully programmable, individually addressable and controllable actuators.

The arrayed actuators described herein are deformable microstructures that curl into and out of the substrate plane. The curling of the actuators is due to the different coefficients of thermal expansion (CTE) of two polyimide layers that make up the structures. An integrated heater resistor is sandwiched between the two polyimide layers. When an electric current is passed through the heater resistor, the temperature of the actuator increases, and the structure (initially deflected out-of-plane) deflects downward into the plane producing both horizontal and vertical displacements. Objects that are placed on the array can be made to move by coordinating the deflections of such actuators.

The purpose of this paper is to describe the first functional ciliary actuator array integrated with CMOS circuitry, providing a means for activating individual cilia and enabling the functions of the array to be altered by software. The overall architecture of the chip and major features are discussed in Section 2. The microfabrication process used to create this ciliary actuator array is described in a separate paper [20]. In Section 3 a description is given of the supporting hardware and software components that are needed to operate the ciliary array chip as a general-purpose manipula-

*This work was performed at the Transducers Lab, Dept. of El. Eng., Stanford Univ. Current address: Xerox PARC, 3333 Coyote Hill Rd., Palo Alto, CA 94304, jwsuh@parc.xerox.com.

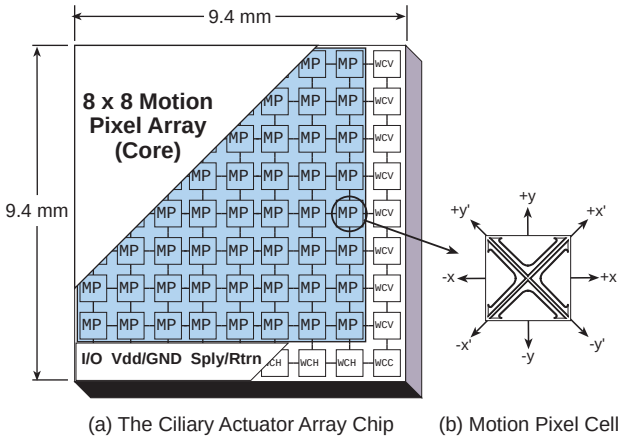

(a) The Ciliary Actuator Array Chip (b) Motion Pixel Cell

Figure 1: The general architecture of the CMOS ciliary array is illustrated at left. Surrounding the 8×8 motion pixel (MP) cells are various circuits for input and output (I/O) of data, clocking, and power. The peripheral circuits contain a shift register chain which allows for both serial and parallel methods of loading data in the core. Each motion pixel cell (illustrated at right) has four triangle-shaped ciliary actuators.

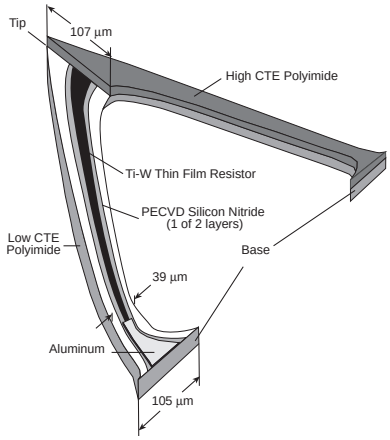

Figure 2: Illustration of the polyimide-bimorph thermal ciliary microactuator. In plan view (see Figure 1b), the actuator has the shape of two sides of an isosceles triangle. The base of the actuator is attached to the substrate at two locations. In this illustration, half of the upper polyimide and PECVD silicon nitride layers are shown removed to reveal the middle layers.

tion tool. Section 4 provides results on the manipulation array that was used to move a silicon die. Finally, a summary of these results is provided in Section 5.

2 System Architecture

2.1 Chip Architecture

The general architecture of the CMOS integrated ciliary array chip is shown in Figure 1a. The device is composed of two basic sections: the array core and the periphery surrounding the array core on two sides. The array core consists of 256 ciliary actuators each with their associated logic and driver circuitry. The actuators are grouped into 64 1mm $\times$ 1mm cells (Figure 1b) and are arranged as an 8×8 array. Along the periphery of the core is a shift register chain, a mode select circuit, and row and column data loading circuits. The shift register chain consists of 16 cells, each of which has a shift register and a serial-parallel/row loader. These circuits provide the option of loading data into the individual cilia in a parallel or serial manner. The periphery also contains the voltage and ground bond pads for the logic circuits (Vdd/Gnd) and the power supply and return bond pads for the ciliary actuators. There are also eight sets of *Supply* and *Return* pads located in the horizontal wiring cells (one set per motion pixel column) to provide for a separate power supply voltage for the actuators (potentially above the logic supply).

2.2 Motion Pixel Cells

The four ciliary actuators in each motion pixel are arranged orthogonally in a common-tip configuration. Each cilium has a driver circuit consisting of logic circuits and current drivers. In addition, the motion pixel cell has globally routed power and data interconnect lines that run parallel to its vertical and horizontal axes. Two series connected D-flip-flops (or phase registers) provide a buffering scheme so that one register can be updated while the other register is controlling the actuator state. This arrangement enables simultaneous updating of all cilia. A register transfer signal enables the second register to change its state, thus transferring new data to the buffers and the MOSFET current driver.

The ciliary actuator is a triangle-shaped structure fabricated using surface micromachining. The actuator is a multilayered structure made up of polyimide, silicon nitride, aluminum, and Ti-W films. Figure 2 is an illustration of the actuator with the upper polyimide and silicon nitride layers removed showing the relative placement of the other layers. The width of the cilium varies along its length: at the tip the beam is 107μm wide and gradually tapers to a width of 39μm near the base; at the base the actuator again widens to 105μm. The Ti-W heater resistor ($\approx 1000\Omega$) gradually widens from 10μm near the base to 28μm at the tip. The resistor is widest at the tip area to limit power dissipation and to lessen current crowding effects where the path of the resistor turns through 90°.

2.3 Input/Output Cells

The peripheral cells contain voltage and ground pads and circuits that perform vital input and output (I/O) functions: row and column selection, serial data input/output pads, and cilia selection. The most important function performed by these peripheral cells is serial row and column selection which is accomplished by the 16-cell shift register chain that is routed around two edges of the array core.

3 Experimental Setup

A custom designed printed circuit board (PCB) was made to package the ciliary array chip and to provide the interface between the chip and the controlling personal computer (PC) system. The circuit board was designed to accommodate up to four ciliary array chips. More details of this system hardware are described in a separate paper [20].

Except for the voltage input settings, the ciliary array chip is completely under software control. Diagnostic software was first used to verify that each motion pixel could be individually controlled. The major function of the software is to regulate the gait sequences or to alter the way the actuators induced translation. It also allows the array to be subdivided into smaller fields that are needed for doing vector field manipulations. Having the chip under software control enables an unprecedented level of flexibility in operating a MEMS ciliary actuator array. A variety of low and high-level software functions have been programmed for both linear translation and squeeze field based manipulations [5].

An actuator moves only if the data bit in its corresponding phase register was changed. Therefore, the actuators requires a continuous flow of control signals. In general, these signal sequences consist of address data, motion pixel data, and clock signals, which all depend on the intended array vector field. The software writes a specific sequence of signals to the parallel port in real time.

Software for the higher level functions allows the user to manipulate an object in a preprogrammed or in an interactive manner. Several useful control strategies are preprogrammed and can be chosen from a menu including linear translations for moving a part in the up, right, left, or down direction and vector fields for orienting a part along a vertical or horizontal squeeze line. For each of these strategies, a sequence of control signals is repeatedly written to the parallel port and can consist of many hundreds of individual byte signals.

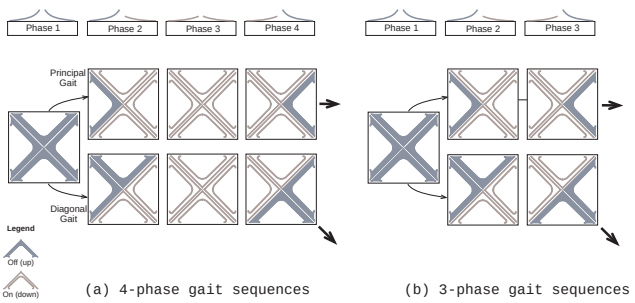

Figure 3: Illustration of different gaits: (a) 4-phase gaits. (b) A new 3-phase gait that omits one of the phases in the 4-phase gait. Standard gaits are shown on the top, virtual (diagonal) gaits on the bottom.

Motion in arbitrary directions can be induced by alternating gaits that interleave gaits of different principal directions. For example, a translation at 25° from the x-axis requires motion in the y-direction and x-direction at a ratio of $\tan 25° \approx 1 : 2$. The control software determines the exact alternation for any translation angle analogously to the Bresenham line scan algorithm [8], resulting in different fields that are interleaved in time. This results in an interactive mode in which the user can, through keyboard commands, move an object at any speed and along any vector.

4 Experimental Results

All five test modules worked as expected, and the power required to achieve full deflection ranged from 35mW to 38 mW (input voltage range: 6.0V to 6.3V; input current range: 5.5mA to 6.4mA).

4.1 Simple Translation Experiments

Linear translation with principal gaits. Several sample parts were used in this experiment, however, the best results were obtained with a 3mm × 3mm × 0.1mm silicon die (from wafers supplied by Virginia Semiconductor, Inc., Fredericksburg, VA) of mass 1.7mg. The heaviest object moved was a 3mm × 3mm × 0.5mm silicon die (8.6mg). Video images of this demonstration are shown in Figure 4. The original FEM simulations indicated that the actual lifting capacity was $\approx 80\mu$N; however, these experiments indicate that the lifting capacity is less than estimated. To move the Si die, each actuator received about 35mW of power. Since at the motion pixel level the principal 4-phase gait has a 75 percent duty cycle, the total average power consumed by the entire array per gait was 6.7W (see Figure 3a). A new 3-phase gait (Figure 3b)

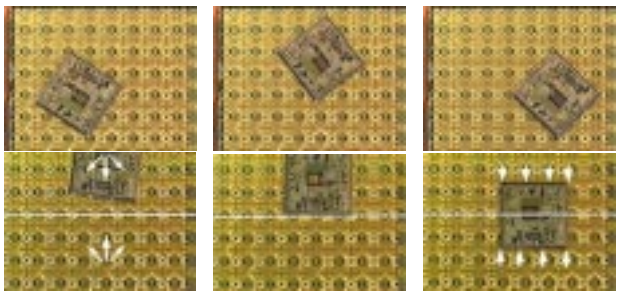

Figure 4: The top three images are frames from a video taken during arbitrary linear translation tests with 4-phase standard gaits. These photos show that along with translation there is slight rotation that is not intended.
The bottom three images are from a video taken during a squeeze field manipulation test. Two diagonal gaits are used to produce a net perpendicular motion to the horizontal squeeze line (see left video image).The middle-bottom frame shows the part about to make contact with the opposing linear field. Right-bottom frame shows the part in rotational and translational equilibrium about the squeezeline.
The video is available online at www.cs.dartmouth.edu/∼brd/Research/MEMS/ciliaarrays.html.

reduces the duty cycle to 67 percent. This gait was also successfully implemented.

Diagonal translation with virtual gaits. The secondary method of moving an object was using a 4-phase gait along the array's diagonals (e.g., Top-Right or Bottom-Left) and applying the appropriate gait pattern (see Figure 3). Since two actuators were commanded to act synchronously, diagonal gaits done in this way are also called virtual gaits because two actuators are working together as one. In this experiment, the actuators again received about 35mW of power, and the total average power consumed by the entire array (per gait) was 5.0W. This pattern uses less power than the principal gait due to the fact that its duty cycle for actuator hold-down is 50 percent (33 percent for 3-phase gait).

It was observed that the motion induced by the virtual gaits was of a higher quality (smoother and faster) than the standard gait. Since using the action of two cilia to move an object effectively doubles the lifting capacity, the quality of induced motion is higher than the standard 4-phase gait.

4.2 Vector Field Experiments

Previous work has introduced *programmable force fields (PFF's)* as a means of controlling actuator arrays in a task-level fashion [7, 5]. PFF's represent

Figure 5: (a) Simulation of the alignment task with a unit squeeze field. Simulation techniques as well as geometric analysis were implemented to demonstrate how the manipulation of small parts can be automatically planned and controlled.
(b) Unstable square-shaped part in a skewed squeeze field ($\epsilon = -1$). The square with center on the squeeze line will rotate indefinitely. Moreover, it has *no* stable equilibrium in this field.

a general tool to model *distributed manipulation* [2]. Here we briefly summarize the most important concepts that form the basis for the new results presented in the remainder of this section.

Consider the following family of control strategies called *squeeze fields*, and a manipulation planning algorithm for parts positioning and orientation. A squeeze field f is a two-dimensional force vector field in which, at each point, a unit force points perpendicularly towards a straight line l (the "squeeze line"). On l the force is zero. See Figure 5a.

Assuming quasi-static motion, an object will translate and rotate to an equilibrium configuration, as characterized in Fig. 5a. To predict the equilibria, a uniform force distribution over the surface of P is assumed, which is an appropriate model for a flat part that is in contact with a large number of elastic actuators.

It was shown in [5] that any polygonal part P has $E = O(rn^2)$ orientation equilibria, where r is the maximum number of edges that a bisector of P can cross. If P is convex, then the number of equilibria is $O(n)$. Equilibria can be calculated numerically or, for polygonal parts, analytically. The following theorem gives a general result on force vector fields [5].

Theorem 1 *Let P be a polygon with n vertices whose interior is connected. There exists a sensorless alignment strategy consisting of a sequence of squeeze fields that uniquely orients P up to symmetries. The sequence has $O(E) = O(n^2 r)$ steps and can be computed in $O(E^2)$ time.*

4.2.1 Task: Orienting and Aligning Parts

If a part is placed in a squeeze field, it will translate and rotate until a stable equilibrium is reached. Parts may exhibit several equilibria, hence after one squeeze

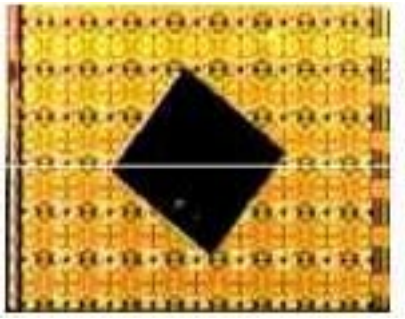

Figure 6: A 3mm × 3mm × 0.1mm square die after reaching stable equilibrium in a squeeze field. The squeeze line is drawn in white.

the part orientation may be ambiguous. This ambiguity can be removed with the strategies of Claim 1: by executing a sequence of squeezes at particular angles, the part is uniquely oriented (see [5]). Note that this task, as well as all those described below, are sensorless, i.e., they do not require sensor feedback.

Squeeze fields. To carry out this task the ciliary array was subdivided into two fields each consisting of either a 4×8 (vertical squeeze line) or 8×4 (horizontal squeeze line) array of motion pixel cells. Squeeze fields with both principle and diagonal direction gaits were implemented. The diagonal gaits had equal proportions $\pm 45^\circ$ to produce a net translation towards the squeeze line.

Various silicon chips were placed near the edge of the ciliary array at the beginning of the experiment. The squeeze field pushed the chips towards the center. Both centering and orienting was observed in good agreement with the predictions from theory and simulation. For square parts two kinds of equilibria were observed: (1) square diagonal coinciding with the squeeze line, and (2) central axis coinciding with the squeeze line. Equilibrium (1) is predicted from the theory of (continuous) force fields. In ideal continuous fields, (2) is an unstable equilibrium. However, Luntz et al. [15, 16] showed that for actuator arrays with discrete contacts, (2) may become a stable equilibrium. These experimental observations indicate that effects from the discrete character of the ciliary array are significant.

Images from the video taken during these experiments are shown in Figure 6, which shows a square part after reaching a stable equilibrium in category (1), and also in Figure 4, which shows a part as it reaches and equilbrium in category (2). In our experiments, the equilibria in category (1) were achieved more frequently.

4.2.2 Task: Centering

Squeeze fields achieve a centering effect only along one axis. Radial fields can center a part in two dimensions. These fields are discussed in this section.

Radial fields. A radial field R is a two-dimensional force vector field such that $R(\mathbf{z}) = -\mathbf{z}/|\mathbf{z}|$ if $\mathbf{z} \neq 0$, and $R(\mathbf{0}) = \mathbf{0}$. A radial field has a potential, $U(\mathbf{z}) = |\mathbf{z}|$.

Claim 2 *Given a polygonal part P in a radial field R, there exists a unique* pivot point *v of P such that P is in equilibrium if and only if v coincides with the center of the radial field. v is typically* not *the center of mass of P.*

Claim 3 *Let P be a polygonal part with n vertices, and let r be the maximum number of edges that a bisector of P can cross. There are at most $E = O(rn)$ stable equilibria in a field of the form $R + \delta S$ if S is a squeeze field, and δ is sufficiently small and positive.*

Proofs of the previous claims, and a numerical algorithm to compute the pivot point is given in [5]. Note that Claim 3 results in strategies for unique part posing in $O(E^2) = O(r^2 n^2)$ time.

Radial fields can be used to center a part. The previous generation four-quadrant cilia device [6] implemented an approximation of an ideal radial field where each quadrant pushes diagonally towards the center. Note that this approximate radial field has a potential whose shape is in the form of an upside-down square pyramid.

With the current fully addressable design a single cilia array suffices to generate such a radial field. Parts centering was demonstrated in recent experiments with (among others) a 3mm × 3mm × 0.1mm chip.

4.2.3 Task: Rotation

Squeeze fields and radial fields cause stable equilibria in parts placed into them. The previous sections exploited this effect to perform open-loop positioning and orienting strategies, and to predict the final pose of a part. However, an equally useful task might be the continuous translation and rotation of a part, for example for inspection of micro-parts under a microscope. This is the focus of the next paragraphs.

Four-quadrant circular fields. A field that causes rotation was described by [9] and [14]. The four quadrants generate forces in East, South, West, and North directions, creating a discretized vortex. The cilia array was programmed to implement this field. Note that this field also has a centering effect which was observed in the experiment.

Skewed squeeze fields. A *skewed field* f_S is a vector field given by $f_S(x, y) = -\text{sign}(x)(1, \epsilon)$, where $\epsilon \in \mathbb{R}\backslash\{0\}$. No skewed squeeze field has a potential [5]. In a skewed squeeze field, it is easy to find a circular path along which the work integral is non-zero (e.g., along a circle with center on the squeeze line). A skewed field induces *no* stable equilibrium on a disk-shaped part (for all $\epsilon \neq 0$, see [5]). Translational equilibrium is only possible if the center of the disk coincides with the squeeze line. In this position the disk experiences a non-zero moment if $\epsilon \neq 0$. Finally, a diagonally skewed field ($\epsilon = \pm 1$) induces *no* stable equilibrium on a square-shaped part [5].

According to the dynamic model above, certain parts will rotate indefinitely in skewed squeeze fields (Figure 5b). Note that even though the cilia device has more degrees of freedom, two areas of constant force are sufficient to implement a skewed field, resulting in a very simple task-level rotation strategy. In particular, the rotation algorithm resulting from the application of skew-symmetric squeeze fields is considerably simpler than previous rotation algorithms (for example, the vortices suggested by [9] or by [14] as described above). While vortices require at least four areas of the array to be pushing in different directions, skewed fields perform the same task with only two regions of constant force.

Diagonal gaits are a particularly simple and effective means to implement skewed fields. The array is subdivided into two rectangular areas with opposing diagonal gaits. For example, if the left half pushes in SE direction, and the right half pushes in NW direction, we obtain a skewed field with $\epsilon = -1$, which causes a counterclockwise rotation (see again Figure 5b).

Skewed squeeze fields were implemented both with the previous and with the new array design. While the former suffered from the fact that the rotation occurred essentially on top of the gap between two separate cilia chips, the new chip was able to implement a full skewed squeeze field on a single array. This resulted in a much smoother rotation motion as well as in an increase in speed by about a factor 10. 360° rotation was possible in less than 1 minute.

4.2.4 Task: Unique Positioning with Universal Fields

Recently it was shown that there exist families of force fields that generate *unique* equilibria for all non-symmetric parts [3].

A combined radial gravity field is defined as $f_\delta(x, y) = R(x, y) + \delta G$ where R is a radial field as defined above, $G = (0, -1)$ is a unit "gravity" field in the $-y$ direction, and $0 \leq \delta \leq 1$.

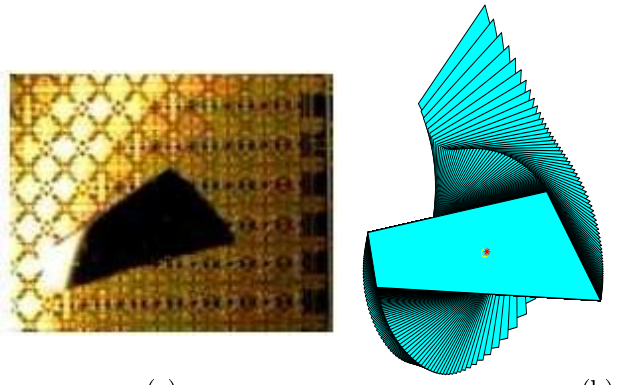

(a) (b)

Figure 7: A "universal field" implemented with a cilia array. (a) In preliminary experiments, the quadrilateral silicon chip was placed on the array implementing a radial field. When the array was tilted to the right, the part consistently reached the same equilibrium from arbitrary initial configurations. (b) Simulation run of the quadrilateral part in the universal field $R + 0.5G$, which corresponds to a tilt angle of approximately $\phi = 30°$.

Claim 4 [3] *Let P be an arbitrary non-symmetric polygonal part. There exists a δ such that P has a unique equilibrium in f_δ.*

This result may give rise to a new generation of parts feeding and positioning devices that do not require any hardware adjustments when the part design is changed, nor do they require sensor feedback or programming.

Tilted radial fields. A "universal field" was implemented for the first time with the cilia array. The radial component was generated with a unit radial field R as described above. To add the gravity component δG, the array was tilted by a small angle ϕ. A nonsymmetric quadrilateral part was used (part sides approximately 1.1mm, 5.3mm, 2.5mm, and 4.3mm, thickness 0.1mm) for these experiments. Initially, for $\delta = 0$ no unique equilibrium was observed. Preliminary experiments showed that by a tilt angle of a few degrees, the part always settled in the same equilibrium.

In Figure 7a the quadrilateral part has reached a stable equilibrium on the tilted cilia array. Figure 7b shows the corresponding simulation with a field $R + 0.5G$. Reasons for the discrepancy between equilibrium orientations in simulation and experiment may include an inaccurate estimate of the δ factor, as well as variations in the performance of the individual actuators, and the relatively small number of discrete actuators in contact with the quadrilateral chip.

5 Summary

The ciliary chip described herein is the first micromanipulation array fabricated directly on top of control circuits. This degree of integration enables each actuator to be separately addressable and turns the array into a reconfigurable micromanipulation device. The design of the previous ciliary array described in [21] limited it to performing linear translations. The current array was designed to perform vector field manipulations such as orienting, alignment, and centering in addition to arbitrary linear translations without having to tile chips together as was done with the previous arrays.

Realization of this ciliary array was carried out by surface micromachining polyimide-based actuators on substrates with pre-fabricated CMOS circuits. Only a few chips needed to be packaged for the tests in this paper because the operational yield was excellent. Over all the chips tested, only a few motion pixels exhibited less than expected performance during operation. No problems due to thermal degradation such as loss of adhesion between layers was observed during testing.

Validation of this approach was achieved through the demonstration of the chip with individual motion pixels, simple uniform vector fields, or subdivided vector fields. Translation along arbitrary vectors and squeeze field centering and alignment were successfully demonstrated, as well as centering with a radial field. Preliminary experiments on a "universal parts feeder" were also performed successfully.

Acknowledgments

The authors thank all the staff of the Stanford Nanofabrication Facility (SNF) for their professional and dedicated service. We thank the students, staff, industrial affiliates, and visiting scholars of the Stanford Transducers Lab for their encouragement and fruitful discussions over the course of the entire organic bimorph actuators research project. Particular thanks go to Aaron Partridge, Ken Honer, Bart Kane, and Jitendra Mohan for their development of a reliable CMOS process at the SNF. The valuable help of Trevor Barcelo and Brian Epplett during the processing of these chips is greatly appreciated.

Support for the ciliary array chip research was initially provided by DARPA (No. N001-92-J-1940-P00001) and last two years were provided by a General Motors Key grant and Kovacs' NSF NYI award (ECS-9358289-006). Research on programmable vector fields was provided in part by several NSF grants to Donald (IRI-8802390, IRI-9000532, IRI-9530785, NSF 9802068, NSF CDA-9726389, NSF EIA-9818299, NSF CISE/CDA-9805548, NSF IRI-9896020, IIS-9906790, and EIA-9901407), by a Presidential Young Investigator award to Donald, by an NSF/DARPA Small Grant for Exploratory Research (IRI-9403903), by an NSF CISE Postdoctoral Associateship No. CDA-9705022 and an NSF CAREER award No. ECS-9875367 to Karl Böhringer, and in in part by the Air Force Office of Scientific Research (AFSOR), the Mathematical Sciences Institute, Intel Corporation, and AT&T Bell Laboratories; and in part by DARPA (DABT63-69-C-0019).

References

[1] M. Ataka, A. Omodaka, and H. Fujita. A biomimetic micro motion system. In *Transducers — Digest Int. Conf. on Solid-State Sensors and Actuators*, pages 38–41, Pacifico, Yokohama, Japan, June 1993.

[2] K. F. Böhringer and H. Choset, editors. *Distributed Manipulation*. Kluwer Academic Publishers, Boston/Dordrecht/London, 2000. ISBN 0-7923-7728-1.

[3] K.-F. Böhringer, B. R. Donald, L. Kavraki, and F. Lamiraux. Part orientation with one or two stable equilibria using programmable vector fields. *IEEE Transactions on Robotics and Automation*, 2000. Forthcoming.

[4] K.-F. Böhringer, B. R. Donald, and N. C. MacDonald. Single-crystal silicon actuator arrays for micro manipulation tasks. In *Proc. IEEE Workshop on Micro Electro Mechanical Systems (MEMS)*, pages 7–12, San Diego, CA, Feb. 1996.

[5] K.-F. Böhringer, B. R. Donald, and N. C. MacDonald. Programmable vector fields for distributed manipulation, with applications to MEMS actuator arrays and vibratory parts feeders. *Int. Journal of Robotics Research*, Feb. 1999.

[6] K.-F. Böhringer, B. R. Donald, N. C. MacDonald, G. T. A. Kovacs, and J. W. Suh. Computational methods for design and control of MEMS micromanipulator arrays. *IEEE Computer Science and Engineering*, pages 17–29, January–March 1997.

[7] K.-F. Böhringer, B. R. Donald, R. Mihailovich, and N. C. MacDonald. A theory of manipulation and control for microfabricated actuator arrays. In *Proc. IEEE Workshop on Micro Electro Mechanical Systems (MEMS)*, pages 102–107, Oiso, Japan, Jan. 1994.

[8] J. D. Foley, A. Van Dam, Feiner, and Hughes. *Computer Graphics: Principles and Practice*. Addison Wesley, Reading, MA, 2nd edition, 1996.

[9] H. Fujita. Group work of microactuators. In *International Advanced Robot Program Workshop on Micromachine Technologies and Systems*, pages 24–31, Tokyo, Japan, Oct. 1993.

[10] T. Furuhata, T. Hirano, and H. Fujita. Array-driven ultrasonic microactuators. In *Transducers — Digest Int. Conf. on Solid-State Sensors and Actuators*, pages 1056–1059, Montreux, France, June 1991.

[11] S. Konishi and H. Fujita. A conveyance system using air flow based on the concept of distributed micro motion systems. *Journal of Microelectromechanical Systems*, 3(2):54–58, 1994.

[12] S. Konishi, Y. Mita, and H. Fujita. Autonomous distributed system for cooperative micromanipulation. In K. F. Böhringer and H. Choset, editors, *Distributed Manipulation*, pages 87–102. Kluwer Academic Publishers, Boston/Dordrecht/London, 2000. ISBN 0-7923-7728-1.

[13] C. Liu, T. Tsai, Y.-C. Tai, W. Liu, P. Will, and C.-M. Ho. A micromachined permalloy magnetic actuator array for micro robotics assembly systems. In *Transducers — Digest Int. Conf. on Solid-State Sensors and Actuators*, volume 1, pages 328–331, Stockholm, Sweden, June 1995.

[14] W. Liu and P. Will. Parts manipulation on an intelligent motion surface. In *IEEE/RSJ Int. Workshop on Intelligent Robots & Systems (IROS)*, volume 3, pages 399–404, Pittsburgh, PA, Aug. 1995.

[15] J. E. Luntz, W. Messner, and H. Choset. Velocity field design for parcel positioning on the virtual vehicle, a discrete distributed actuator array. In P. K. Agarwal, L. Kavraki, and M. Mason, editors, *Robotics: The Algorithmic Perspective*. A. K. Peters, Ltd, Wellesley, MA, 1998.

[16] J. E. Luntz, W. Messner, and H. Choset. Discreteness issues in actuator arrays. In K. F. Böhringer and H. Choset, editors, *Distributed Manipulation*, pages 103–126. Kluwer Academic Publishers, Boston/Dordrecht/London, 2000. ISBN 0-7923-7728-1.

[17] Y. Mita, S. Konishi, and H. Fujita. Two dimensional micro conveyance system with through holes for electrical and fluidic interconnection. In *Transducers — Digest Int. Conf. on Solid-State Sensors and Actuators*, volume 1, pages 37–40, Chicago, IL, June 1997.

[18] H. Nakazawa, Y. Watanabe, and O. Morita. The two-dimensional micro conveyor: Principles and fabrication process of the actuator. In *Transducers — Digest Int. Conf. on Solid-State Sensors and Actuators*, volume 1, pages 33–36, Chicago, IL, June 1997.

[19] K. S. J. Pister, R. Fearing, and R. Howe. A planar air levitated electrostatic actuator system. In *Proc. IEEE Workshop on Micro Electro Mechanical Systems (MEMS)*, pages 67–71, Napa Valley, California, Feb. 1990.

[20] J. W. Suh, R. B. Darling, K.-F. Böhringer, H. Baltes, B. R. Donald, and G. T. A. Kovacs. CMOS integrated organic ciliary array for general-purpose micromanipulation tool for small objects. *Journal of Microelectromechanical Systems*, 8(4):483–496, Dec. 1999.

[21] J. W. Suh, S. F. Glander, R. B. Darling, C. W. Storment, and G. T. A. Kovacs. Organic thermal and electrostatic ciliary microactuator array for object manipulation. *Sensors and Actuators A (Physical)*, 58:51–60, 1997.

[22] N. Takeshima and H. Fujita. Polyimide bimorph actuators for a ciliary motion system. In *ASME WAM Symposium on Micromechanical Sensors, Actuators, and Systems*, volume DSC-32, pages 203–209, 1991.